Materials Science & Engineering C 122 (2021) 111928

Contents lists available at ScienceDirect

Materials Science & Engineering C

journal homepage: www.elsevier.com/locate/msec

Engineering 3D printed bioactive composite scaffolds based on the combination of aliphatic polyester and calcium phosphates for bone tissue regeneration

Eduardo H. Backes [a,b,*], Emanuel M. Fernandes [b,c,**], Gabriela S. Diogo [b,c], Catarina F. Marques [b,c], Tiago H. Silva [b,c], Lidiane C. Costa [a], Fabio R. Passador [d], Rui L. Reis [b,c], Luiz A. Pessan [a]

[a] Graduate Program in Materials Science and Engineering, Federal University of São Carlos, via Washington Luiz, Km 235, 13565-905 São Carlos, SP, Brazil
[b] 3B's Research Group, I3Bs – Research Institute on Biomaterials, Biodegradables and Biomimetics, University of Minho, Headquarters of the European Institute of Excellence on Tissue Engineering and Regenerative Medicine, AvePark, Parque de Ciência e Tecnologia, Zona Industrial da Gandra, 4805-017, Barco, Guimarães, Portugal
[c] ICVS/3B's – PT Government Associate Laboratory, Braga, Guimarães, Portugal
[d] Science and Technology Institute, Federal University of São Paulo, Talim St. 330, 12231-280 São José dos Campos, SP, Brazil

ARTICLE INFO

Keywords:
Biodegradable polymer
Hydroxyapatite
β-TCP
Bioactive composites
Additive manufacturing
Fused deposition modeling

ABSTRACT

In this study, polylactic acid (PLA) filled with hydroxyapatite (HA) or beta-tricalcium phosphate (TCP) in 5 wt% and 10 wt% of concentration were produced employing twin-screw extrusion followed by fused filament fabrication in two different architectures, varying the orientation of fibers of adjacent layers. The extruded 3D filaments presented suitable rheological and thermal properties to manufacture of 3D scaffolds envisaging bone tissue engineering. The produced scaffolds exhibited a high level of printing accuracy related to the 3D model; confirmed by micro-CT and electron microscopy analysis. The developed architectures presented mechanical properties compatible with human bone replacement. The addition of HA and TCP made the filaments bioactive, and the deposition of new calcium phosphates was observed upon 7 days of incubation in simulated body fluid, exemplifying a microenvironment suitable for cell attachment and proliferation. After 7 days of cell culture, the constructs with a higher percentage of HA and TCP demonstrated a significantly superior amount of DNA when compared to neat PLA, indicating that higher concentrations of HA and TCP could guide a good cellular response and increasing cell cytocompatibility. Differentiation tests were performed, and the biocomposites of PLA/HA and PLA/TCP exhibited earlier markers of cell differentiation as confirmed by alkaline phosphatase and alizarin red assays. The 3D printed composite scaffolds, manufactured with bioactive materials and adequate porous size, supported cell attachment, proliferation, and differentiation, which together with their scalability, promise a high potential for bone tissue engineering applications.

1. Introduction

Poly(lactic acid) (PLA) is an aliphatic polyester that can be sustainably synthesized from natural resources, and it presents a good balance of mechanical properties, as high young modulus and tensile strength, with great biocompatibility and biodegradability, thus receiving great attention by the biomedical community and applied in the fabrication of bioabsorbable surgical sutures, screws, drug delivery systems and guided tissue regeneration [1–3]. Latterly, the advent of additive manufacturing technologies, namely melt-based process as Fused Filament Fabrication (FFF), also expanded PLA consumption through new applications [4–6]. Two of the shortcomings that compromise PLA

* Correspondence to: E. H. Backes, Graduate Program in Materials Science and Engineering, Federal University of São Carlos, via Washington Luiz, Km 235, 13565-905 São Carlos, SP, Brazil.
** Correspondence to: E. M. Fernandes, ICVS/3B's – PT Government Associate Laboratory, Braga, Guimarães, Portugal.
E-mail addresses: ehbackes@gmail.com (E.H. Backes), efernandes@i3bs.uminho.pt (E.M. Fernandes), gabriela.carlos@dep.uminho.pt (G.S. Diogo), catarina.marques@i3bs.uminho.pt (C.F. Marques), tiago.silva@i3bs.uminho.pt (T.H. Silva), lidiane@ufscar.br (L.C. Costa), fabio.passador@unifesp.br (F.R. Passador), rgreis@i3bs.uminho.pt (R.L. Reis), pessan@ufscar.br (L.A. Pessan).

https://doi.org/10.1016/j.msec.2021.111928
Received 18 May 2020; Received in revised form 21 October 2020; Accepted 28 January 2021
Available online 3 February 2021

outspread applications are the low impact toughness, acid wastes release from degradation, and lack of bioactivity [4,7–9]. The last attribute has recently been approached through different manners, particularly by chemical modifications and incorporation of bioactive fillers [10–12]. The melt compounding of PLA is more appropriate for large-scale production, and extrusion is the major consolidated technique to produce these biopolymer composites.

Hydroxyapatite (HA) and β-tricalcium phosphate (TCP) are some of the most investigated and promising materials for developing bioactive polymer composites since they have a chemical composition similar to the mineral part of the bone [13]. Furthermore, both materials have been extensively used in bone implants and dentistry applications due to their excellent biocompatibility and high bioactivity [13–17]. Due to the lower Ca/P ratio, TCP biodegradation process occurs 3 to 12 times faster than HA. Nevertheless, crystallinity degree, porosity, and surface area also play a significant role in biodegradation kinetics [13,14,18]. Recent advances using PLA/HA and PLA/TCP combined with FFF technologies, become possible to address some of the major demands of the PLA scaffolds, particularly the improvement in biocompatibility, mechanical properties, and production of the well-controlled porous structure. Gremare et al. [19] studied 3D printed PLA scaffolds using FFF technology and evaluated the impact of different pore size in the mechanical properties and cell proliferation. The results demonstrated that the mechanical properties were not sensible to pore sizes variation between 150 μm and 250 μm, with the samples presenting good cell viability and spreading. Senatov et al. [17] produced PLA/HA (85/15 wt%) FFF scaffolds with controlled geometry, 30% of porosity, and pore size of 700 μm, incorporating HA increased crack resistance, namely during low fatigue cycles. Moreover, in vivo tests (rabbit model) showed no inflammatory reaction under two months analyses, and the developed biomaterials revealed to be suitable for trabecular bone implants [20].

Orozco-Díaz et al. developed PLA/HA filaments for FFF applications and observed that although it is possible to fabricate filaments up to 20 wt% of HA, as more HA is added, the polymer flow became unstable, and the authors noticed naked eye inconsistencies in the filament diameter and surface. These matters might lead to printing issues, as HA accumulating in the nozzle, clogging, and reduction of printing quality. In contrast, filaments with 5 and 10 wt% of HA did not present these issues [21]. On its turn, Wu et al. [22] produced PLA/HA filaments up to 15 wt % of HA and recreated trabecular bones from human trabecular bone with improved mechanical properties, namely, elastic modulus and compressive strength.

Chen et al. [23] fabricated 3D scaffolds using PLA/nano-hydroxyapatite filaments, and the constructs presented well-controlled pore geometry and supported cell spreading and differentiation when implanted in vivo. Furthermore, Donate et al. [24] printed scaffolds of PLA with TCP and $CaCO_3$ with increased hydrophilicity and surface roughness; and the combination of two different fillers improved cell adhesion and the metabolic activity of SaOS-2 cells. Together with the progress being observed in the development of appropriate printing materials, the FFF technologies associated with image acquisition software makes possible the obtainment of 3D models, which can be printed to fit the patient-specific defect in a personalized medicine approach [25].

Moreover, several studies have been performed recently, however, most of them lack a complete comprehensive analyses from materials development through materials processing, characterization, and in vitro/vivo models to validate its bioactivity. Therefore, the present study describes the development of bioactive PLA-based scaffolds from the biocomposite filament up to the FFF process, aiming to achieve superior mechanical and biological properties for bone regeneration. Both HA and TCP particles in different concentrations were combined with the PLA matrix by extrusion to obtain scalable filaments with controlled diameter, assessing their rheological and thermal properties. Afterward, an additive manufacturing process was employed to develop 3D porous composite scaffolds in two different architectures characterized in terms of morphological properties, mechanical response, bioactivity, and cytocompatibility envisaging bone tissue engineering applications.

Table 1
Compositions of the PLA based filaments developed by extrusion process.

Samples	PLA (wt%)	HA (wt%)	TCP (wt%)
PLA	100	0	0
PLA5HA	95	5	0
PLA10HA	90	10	0
PLA5TCP	95	0	5
PLA10TCP	90	0	10

2. Materials and methods

2.1. Materials

NatureWorks® LLC provided the aliphatic polyester PLA 2003D (Ingeo™ 2003D, USA), melt flow index (MFI) of 6.0 g/10 min (210 °C, 2.16 kg). Hydroxyapatite was supplied by Sigma Aldrich® (reference number 21223, USA), purity >90% and $d_{50} = 3.7$ μm. The β-tricalcium phosphate (TCP) was provided by Fluidnova (Nanoxim TCP200, Portugal), purity >90%, and $d_{50} = 6.2$ μm. The surface area of dried HA and TCP was determined using Brunauer, Emmett, and Teller method (BET) and nitrogen as adsorption gas. The analysis (n = 2) was performed in a gas sorptometer (Gemini 370, Micromeritics, USA).

2.2. PLA/HA and PLA/TCP filaments production

PLA, PLA/HA, and PLA/TCP filaments were prepared using twin-screw extrusion process. Prior to compounding, PLA was cryogenically milled and dried at 80 °C under vacuum for 4 h. Afterward, dried PLA was mixed with the weighed HA and TCP, homogenized prior adding to the hopper, and processed using a co-rotating screw extruder (MT19TC, BP Process Equipment and Systems LLC,USA), screw diameter of 19 mm and L/D = 25. The temperature profile used for extruding the filaments was set from the hooper to the die zone ranging from 180 °C up to 200 °C, and the screw speed was set constant at 30 RPM. The speed of the puller roller in the take-up unit was adjusted, aiming to control the filament thickness to 1.75 mm. Table 1 presents the different processed compositions based on PLA matrix with different contents of HA and TCP to obtain filament for the FFF process.

2.3. Rheological characterization

The rheological behavior of the pure PLA, PLA/HA, and PLA/TCP was evaluated under low and high shear rates. In the first case, the analysis was conducted in a controlled stress gauge (model AR G2, TA Instruments, USA) with a parallel plate, geometry of 25 mm, and a gap distance between plates of 1 mm, using a permanent regime under an inert nitrogen atmosphere. The tests were conducted at 190 °C from 0.01 to 100 s^{-1}. The rheological characterization at high shear rates was conducted in a capillary rheometer (model 4467, Instron, UK) at 190 °C and the geometry used was: capillary diameter 1 mm, L/R 10, 20, and 30, and the data was corrected by using Rabinowitch correction. Viscoelastic properties were determined under oscillatory regime, and the tests were performed using the same conditions for shear rates, however, for this analysis, the deformation was limited from 0.1 to 10%, within the linear viscoelastic limit of each material, and the storage (G′) and loss modulus (G″) were analyzed over angular frequency from 0.1 to 500 rad s^{-1}.

2.4. Gel permeation chromatography (GPC)

GPC was performed on the PLA, PLA/HA, and PLA/TCP filaments, the samples were dissolved in tetrahydrofuran (THF) at 50 °C, filtered,

and analyzed using a GPC (Viscotek HT Module 350a, Malvern Instruments, UK) at a pump flow of 1 mL min^{-1}. The GPC calibration curves were obtained from polystyrene (PS) standards.

2.5. Thermal characterization

The thermal characterization of the developed composite filaments was performed by using differential scanning calorimetry (DSC) and thermogravimetric analyses (TGA).

DSC was used to assess the glass transition temperature (T_g) and evaluate the impact on the thermal properties by incorporating HA and TCP in different concentrations. The effect of the fillers in the crystallization behavior of PLA was also addressed. The DSC analysis was conducted in a TA Instruments equipment (model QS100, USA), using nitrogen in a continuous flow of 50 mL min^{-1}. The T_g value of the samples was obtained at the second heating cycle, and the samples were tested in triplicates. Samples were initially heated from 0 °C to 200 °C at a heating rate of 10 °C min^{-1}, then cooled down to 0 °C and reheated to 200 °C at a heating rate of 10 °C min^{-1}. The degree of crystallinity (χ_c) was determined according to Eq. (1):

$$\chi_c = \frac{\left(\Delta H_{melt} - \Delta H_{cold\ cryst}\right)}{H_\infty * \left(1 - \frac{Filler\ wt\%}{100}\right)} \quad (1)$$

where ΔH_{melt} is the enthalpy of melting of the sample, $\Delta H_{cold\ cryst}$ is the enthalpy of cold crystallization, H_∞ is the theoretical melting temperature of the PLA 100% crystalline (93.7 J/g), and *filler wt%* corresponds to the amount of HA or TCP in the composite [26].

The thermal stability of the developed filaments was evaluated by thermogravimetry analysis using a TA Instruments equipment (model TGA Q50, USA). The samples were heated from room temperature until 800 °C, using a heating rate of 20 °C min^{-1} under nitrogen atmosphere. Triplicates were made for each sample.

2.6. PLA and composite scaffolds production by FFF

The scaffolds were designed via Solidworks® (Dassault Systemes, USA), and printed using a commercial 3D printer (Sethi S3 3D, Sethi, Brazil). The printing and bed temperatures were 180–190 °C and 50 °C, respectively, and the scaffolds were manufactured at a printing speed of 20 mm s^{-1} using a brass nozzle (diameter of 400 μm). Three different geometries were developed being 0–90°, 0–45°, and 100% filled. The first one was composed of a square of 13 mm by 3.6 mm height, composed of 12 layers of 300 μm height, 400 μm width, space between filaments (pore size) of 200 μm, and 90° rotation between alternated layers, namely geometry 0–90°. The second geometry is composed of the same parameters used in the 0–90°, but the rotation between the second and the first layer is 45°, and the third layer presents a rotation of −45° compared to the first layer, namely geometry 0–45°. In the geometry 0–90°, the pattern is repeated every two layers, and for 0–45° pattern, every three layers.

2.7. Morphological analysis

The morphology of the developed architectures (filament width, height, pore size, and porosity) was assessed by micro-computed tomography (Micro-CT) and by scanning electron microscopy (SEM).

Micro-CT was performed in a lab-based micro-computed tomography (model 1172. SkyScan, Belgium) using spatial resolutions of 5 μm, x-ray voltage of 59 kV, and current of 167 μA, scanning angular rotation of 180° at rotation step of 0.2°.

The theoretical porosity of the scaffolds was calculated using the Eq. (2)

$$Porosity = 1 - \frac{Vsolid}{Vtotal} * 100\ (\%) \quad (2)$$

where, V_{solid} is the volume of the scaffold, and V_{total} the volume determined by the dimensions of the scaffold (L × W × T).

For each scaffold, a rectangle of approximately 9 mm^2 was determined as a region of interest (ROI), and the 3D models were reconstructed and analyzed using the software CTan (SkyScan, ver.1.14, Belgium) and CTvol (SkyScan, ver. 3.0, Belgium). The threshold was adjusted to identify solid and hollow phases, and the porosity was determined by 3D analysis (Batman, Skyscan, Belgium). The Micro-CT technique was chosen for being a non-destructive technique that determines the scaffold's porosity and interconnectivity.

The morphology of the scaffolds, pore size, filament width, and layer height was determined using Scanning Electron Microscopy (SEM) using a JEOL (model JSM-6010 LV, Japan) and a Philips (model XL30 FEG, Germany) operating both at an accelerating voltage of 15 kV. The samples were coated with a thin layer of gold to enable the analysis, and the images were analyzed using ImageJ® (National Institutes of Health, USA), ten measurements were carried out on each sample (n = 3) The dispersion of the HA and TCP was assessed by employing electron dispersive spectroscopy mapping (EDS).

2.8. Mechanical tests

The mechanical characterization of the PLA, PLA/HA, and PLA/TCP scaffolds was performed using uniaxial compression tests according to ASTM D 695-15 on a universal testing machine (model 5569, Instron, UK) using a load cell of 2 kN, pre-load of 1 N, and a crosshead speed of 1.3 mm min^{-1}, until the maximum load of the scaffolds architectures. The compressive stress and strain were recorded for every 100 ms, and the compressive modulus was calculated by the slope of the stress-strain linear region prior to failure (in the range of 10–15%). At least 5 specimens were tested for each composition and one-way ANOVA followed by post hoc Tukey test ($p < 0.05$) was used for the analysis of variance.

2.9. In vitro bioactivity via simulated body fluid (SBF)

Bioactivity test by incubation in SBF was performed, aiming to evaluate the apatite-forming ability of the scaffolds. The assay was conducted according to the ISO 23317, and the samples were soaked in the SBF solution under different times of analyses, 1, 3, and 7 days at 37 °C and SEM was used to assess the apatite formation on the surface of the scaffolds.

2.10. Cell culture and live/dead bioactivity assay of MC3T3

2.10.1. Cell culture

The cell culture and live/dead bioactivity assay were performed to evaluate cell attachment and cytocompatibility in the scaffolds of PLA, PLA/HA, and PLA/TCP for 0–90° geometry. Three different culture times were assessed, 1, 3, and 7 days, according to the following procedure. Briefly, with the aid of a surgical blade, the scaffolds were cut to obtain six equal samples, which were sterilized with ethylene oxide at 45 °C for 4 h and then cultured with preosteoblast cells (MC3T3-E1) in a 48 well-plate. The cells were seeded using a top-down approach, where the cell seeding occurred on the surface of the scaffolds, using a drop of 25 μL with cell density of 25.000 cells and 1 h for cell attachment was allowed before complete each well with final volume of medium of 500 μL Alfa Modified Eagle Medium (α-DMEM, Life technologies, USA) supplemented with 10% v/v of fetal bovine serum (FBS, Life technologies, USA) and 1% v/v of penicillin-streptomycin The culture medium was changed every 2–3 days.

2.10.2. Live/dead qualitative test

The Live/Dead analysis was performed using Calcein AM (ALFAGENE, UK), and Propidium iodide (PI) (ALFAGENE, UK). Calcein is a membrane green fluorescent cell marker, while PI is a red fluorescent nuclei marker commonly used for identifying dead cells. Briefly, the under culture scaffolds were washed with PBS and incubated in the dark for 5 min with 500 μL of α-DMEM and the markers (Calcein AM 1:1000 and PI 1:500). An inverted fluorescence microscope (Axio Imager Z1m, Zeiss, Germany) was used to analyze live and dead cells (1 and 7 days), and the images were obtained sweeping Z-axis (Z stack, 18 μm range, 40 slices).

2.10.3. DNA quantification

Cell proliferation assay was carried out at predefined culturing times, namely, 1,3, and 7 days. Briefly, the scaffolds were collected and washed with PBS, transferred to 1.5 mL tubes, lysed by addition of 1 mL of Milli-Q water, and then frozen at −80 C until use. Prior to the DNA quantification, the tubes with scaffolds were thawed and placed in an ultrasound bath for 30 min at cold water. The DNA analysis was done using a Quant-iT™ PicoGreen® Kit (Alfagene, UK), according to the manufacturer's instructions. The DNA concentration was obtained from DNA standard solutions, and the fluorescence intensity was read at 485/530 (excitation/emission) in a microplate reader (Synergy HT, Bio-Tek, USA). The statistical analyses were performed using one-way ANOVA followed by Tukey test with post hoc ($p < 0.05$).

2.11. Cell culture and differentiation of stem cells

2.11.1. Cell culture

Human adipose-derived mesenchymal stem cells (hASCs) were isolated from samples of liposuction adipose tissue following a protocol established with the Plastic Surgery Department of Hospital da Prelada (Porto, Portugal) [27,28]. All patients gave their consent for inclusion before participating in the study. The protocol was approved by the Hospital da Prelada Ethics Committee (PI N° 005/2019) and by the 3B's Research Group. After isolation, cells were characterized by flow cytometry (FACSCalibur flow cytometer, BD Biosciences, USA) for stem cell surface markers. Briefly, the cells were resuspended in a 3% v/v bovine serum albumin solution incubated for 30 min at room temperature, with anti-human rat antibodies and separated using the following positive surface markers CD34-PE, CD73- PE, CD90-APC, CD105-FITC, and only one negative, CD45-FITC (BD Biosciences, Germany). . The hASCs were expanded in α-MEM medium supplemented with sodium bicarbonate, 10% v/v fetal bovine serum, and 1% v/v penicillin-streptomycin solution. The hASCs cells were expanded and seeded using the same procedure for MC3T3, however higher cell density was used: 50,000 cells and only PLA, PLA10HA, and PLA10TCP were analyzed [29]. One day after seeding, and in order to induce the hASCs differentiation into the osteoblastic lineage, cells were also cultured with osteogenic medium: basal medium supplemented with 10 mM glycerophosphate (Sigma, USA), 1×10^{-6} M dexamethasone (Sigma, USA), and 50 μg/ml ascorbic acid (Sigma, USA). The culture media were changed every 2–3 days during the analysis period (21 days). The Live/Dead and cell proliferation assays were carried out at predefined culturing times, namely, 7,14 and 21 days, following the same procedure described above.

2.11.2. Cell differentiation

Alkaline phosphatase (ALP) quantification was performed according to manufacturer's instructions, and a phosphatase substrate (Sigma-Aldrich, USA) (100 μL) and an alkaline buffer solution 1.5 M (Sigma-Aldrich, USA) were used. The samples were incubated in the dark for 1 h at 37 °C, the reaction was stopped by using 0.3 N of NaOH. The ALP standard curves were obtained from different dilutions of 4-Nitrophenol (Sigma-Aldrich, USA) solution 10 mM, and the absorbance was read at 405 nm. The experiments were conducted using triplicates and three independent experiments were performed. The statistical analyses were performed using one-way ANOVA followed by Tukey test with post hoc ($p < 0.05$).

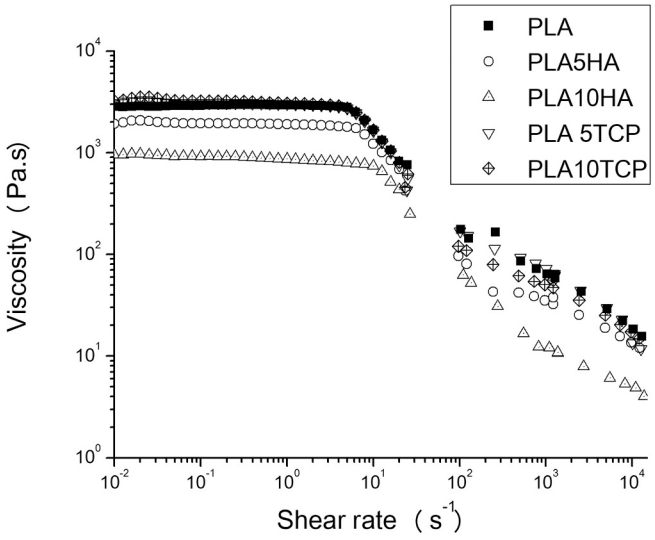

Fig. 1. Viscosity against shear rate for PLA filaments and PLA composites.

Matrix mineralization was analyzed out using alizarin red (AR) staining after 7, 14, and 21 days of cell culture. Briefly, the scaffolds were retrieved, washed with PBS, and fixated with a solution of 10% v/v buffered formalin at 4 °C overnight. Afterward, the samples were washed several times with Milli-Q ® water and incubated in 2% (w/v) of AR (Merck, Germany), pH 4.2–4.3, for 30 min under calm shaking apart of light. Quantitative analyses were performed by extraction of mineralized alizarin crystals using a solution of 10% (w/v) cetylpyridinium chloride (CPC, Sigma-Aldrich®, USA) in 10×10^{-3} M sodium phosphate (Sigma-Aldrich®, USA) for 1 h under shaking. The absorbance was read at 562 in a microplate reader (Synergy HT, Bio-Tek, USA), and the calibration curve was obtained by absorbance of the solution of AR/CPC, and the values of the scaffolds without cells were used as blank. The experiments were conducted using triplicates and three independent experiments were performed. The statistical analyses were performed using one-way ANOVA followed by Tukey test with post hoc ($p < 0.05$).

3. Results and discussion

In this study, polymer extrusion was used to fabricate filaments of PLA and calcium phosphates in a scalable and controlled way. During polymer extrusion, the materials were submitted to high levels of shear strain, which lead to efficacious fillers dispersion. Therefore, by controlling the polymer flow rate and adjusting the take-up speed, filaments controlled to 1.75 mm ± 0.1 mm were obtained.

3.1. Rheological characterization

The fabrication of 3D printed parts comprises several steps, such as image acquisition, filament fabrication, and printing parameters setup. Furthermore, some of the essential printing parameters are correlated to the thermal and rheological characteristics of the materials. For instance, the temperature of printing as well as material viscosity impact in the printing accuracy and limits printing speed since longer times might be necessary for the layers to cool down below a temperature where the filament deformation does not compromise precision, and the layers are still tightly bond [30]. Another aspect is the influence that the addition of fillers has on the thermal and rheological properties in the PLA matrix.

In this study, the rheological properties of neat PLA and those

Table 2
Values of viscosity at a shear rate of 0.01 s^{-1} and macromolecular properties of the PLA, PLA/HA, and PLA/TCP filaments.

Samples	Rheological data	gpc data		
	$\eta_{0@\dot{\gamma}}(0.01\ s^{-1})$*	Mn (g/mol)	Mw (g/mol)	Polydispersity index
PLA Pellet	-	115,000	204,000	1.77
PLA	2817 ± 26	105,000	183,000	1.74
PLA5HA	1943 ± 71	91,000	166,000	1.82
PLA10HA	1056 ± 106	70,000	141,000	2.01
PLA5TCP	3107 ± 85	97,000	173,000	1.78
PLA10TCP	3316 ± 89	94,000	163,000	1.73

* Total mean ± standard deviation.

composite filaments obtained by the extrusion process were assessed by viscosity in the function of the shear rate.

Fig. 1 presents viscosity against shear rate for PLA, PLA/HA, and PLA/TCP composites. As it can be noticed, PLA filament viscosity is not sensible to the increase of shear rate ($\dot{\gamma}$) from 0.01 s^{-1} to 10 s^{-1}, and the viscosity remains constant during the test. However, for the PLA/HA composites, the addition of 5 wt% and 10 wt% of HA lead to a decrease of the viscosity in all the shear rate range analyzed, and higher contents of HA intensified this reduction. Considerable efforts have been made aiming to figure out this behavior presented, and some explanations are that the HA acts reduction the activation energy of PLA thermodegradation, and the calcium can participate in catalyzing nucleophilic substitution reactions [31–34].

Regarding the rheological characterization of PLA/TCP composites, they present similar behavior as of the PLA. Nonetheless, the addition of TCP leads to a slight improvement in the viscosity, and by 10 wt% of TCP, the increase of the viscosity at a low shear rate (1–10 s^{-1}) was approximately 17% higher compared to neat PLA. At high shear rates, PLA and PLA/TCP composites exhibit comparable rheological responses. Moreover, some factors such as purity, surface area, and crystallinity play a significant role during thermal degradation during processing PLA with calcium phosphates. According to the supplier, HA has purity higher than 90%, and it presents metals contents (including iron) ≤ 400 ppm and a specific surface area of approximately 51.7 ± 1.5 m^2/g.

In contrast, TCP presents similar purity and lower metal content ≤20 ppm and a much lower surface area of 1.1 ± 0.1 m^2/g. Metals as iron are known for the ability to catalyze degradation reactions, and since HA has higher metals contents and surface area, the behavior obtained was expected according to the literature [35].

Further information regarding viscoelastic behavior of the filaments under oscillatory regime is presented in Supplementary data Fig. 1.1. In summary the filaments presented similar elastic and viscous component (G′) and (G″), and the relaxation time for all materials in the order of 0.01 s. This result indicates that, during the printing process, after the material leaves the nozzle extruder, the materials remain practically without residual deformation due to the low relaxation time. Table 2 presents the values of viscosity at a shear rate of 0.01 s^{-1} (η_0), and the macromolecular properties of the filament samples, as number average molecular weight (Mn), weight average molecular weight (Mw), and polydispersity index (Mw/Mn).

As presented in Table 2, the process of cryogenically milling and extrusion for filament fabrication does not significantly impact the molecular weight of neat PLA since only a slight detriment (less than 10%) in the molecular weight is observed when compared the pellet of PLA with PLA filament.

Fig. 2 presents the GPC curves for PLA, PLA/HA, and PLA/TCP, respectively. The results presented in Fig. 2a for PLA and PLA/HA samples agree with the results shown previously, where the slight detriment of the molecular weight of PLA/HA composites leads to a reduction of the viscosity baseline. PLA/TCP composites also exhibited a slight decrease in molecular weight; nonetheless, the viscosity baseline increased due to a positive balance due to the physical capacity of the filler to hinder chain mobility and, consequently, their flow.

3.2. Thermal properties

DSC and TGA analyses were performed to evaluate the impact of the HA and TCP on T_g, crystallization behavior of PLA, and its thermal stability. The DSC thermograms are presented in Fig. 3 and their results in Table 3, respectively.

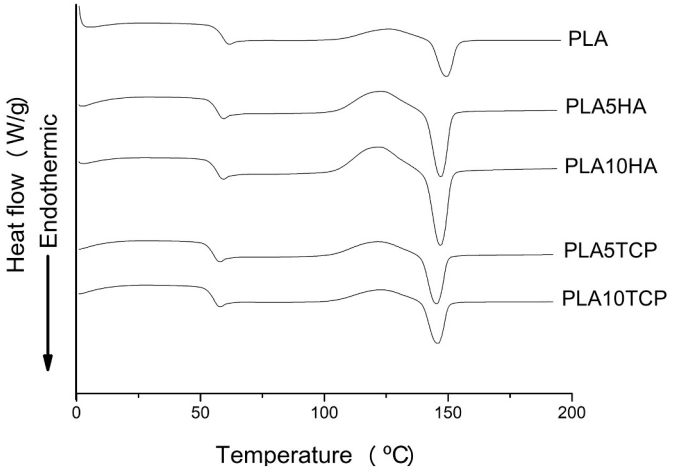

Fig. 3. DSC thermograms for PLA, PLA/HA, and PLA/TCP filaments.

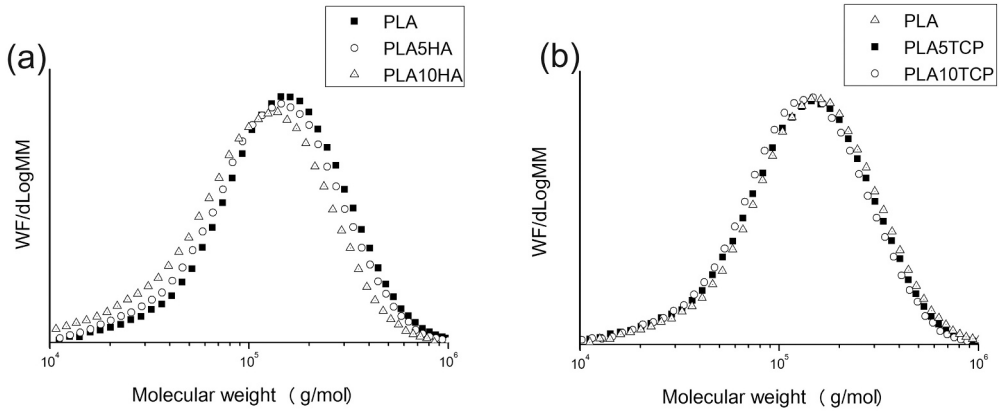

Fig. 2. GPC chromatographs for (a) PLA and PLA/HA, (b) PLA and PLA/TCP (b).

Table 3
DSC results for PLA, PLA/HA, and PLA/TCP composites*.

Samples	T_g (°C)	$\Delta H_{cold\ cryst}$ (J/g)	$T_{melt\ peak}$ (°C)	ΔH_{melt} (J/g)	χ_c (%)
PLA	61.1 ± 0.3	7.2 ± 0.3	150.8 ± 0.2	7.6 ± 0.5	0.4 ± 0.2
PLA5HA	60.1 ± 0.3	13.1 ± 0.3	150.1 ± 0.1	13.3 ± 0.3	0.2 ± 0.1
PLA10HA	59.8 ± 0.8	15.1 ± 0.1	150.0 ± 0.1	15.2 ± 0.1	0.1 ± 0.1
PLA5TCP	58.5 ± 0.4	9.3 ± 0.1	150.2 ± 0.2	9.4 ± 0.1	0.1 ± 0.1
PLA10TCP	58.6 ± 0.2	7.8 ± 0.1	150.1 ± 0.4	8.3 ± 0.3	0.7 ± 0.4

* Total mean ± standard deviation.

The thermograms of Fig. 3 shows that PLA presents non-isothermic cold crystallization, and its maximum rate occurs around 108 °C, and the addition of different contents of HA and TCP did not modify this behavior, therefore no significant changes were observed in T_g or melting peak temperature ($T_{melt\ peak}$). For both composites, the enthalpy of cold crystallization ($\Delta H_{cold\ cryst}$) was higher than for PLA, evidencing that both fillers have the potential to improve nucleation sites for crystallization. Moreover, the degree of crystallinity (χ_c) corresponded to the polymer fraction crystallized during non-isotherm cooling and was below 0.7% for all samples. The low crystallization was expected due to the well-known low kinetics crystallization of PLA [36]. Despite the low crystallinity presented by PLA and PLA composites benefits the production of FFF scaffolds in 2 different ways; namely, for FFF applications, low crystallization degree leads to better printing precision without almost any linear contraction during cooling [30]. Second, because it is described that the biodegradation ratio is related to polymer crystallinity and surface area, being accelerated in amorphous scaffolds with high surface area [36–38].

The TGA was used to evaluate the thermal stability of the filaments and if the addition of fillers might compromise composite's performance. Fig. 4 presents the curves of weight loss in function of temperature for PLA, PLA/HA, and PLA/TCP composites. Table 4 presents the results of TGA analysis, and it can be noticed that once more, the HA and TCP have not changed the thermal properties of PLA significantly. The slight variation observed on the onset of thermal degradation (T_{onset}) of the composites presented and the peak maximum of weight loss (T_{peak}), is within the range of standard deviation. The incorporation of the biofillers in the composites was assessed by analyzing the residue at 800 °C. The results showed that the contents of TCP were more near the proposed and presented lower standard deviation compared to HA and for both composites, the values were corrected subtracting PLA residue at 800 °C. PLA printing temperature was set in the range of 180–200 °C. Therefore, we determined the filament's weight loss from room temperature (RT) until 200 °C, aiming to analyze the thermal stability of them during working conditions. The results showed a weight change lower than 0.2% for the materials and not significant change between composites.

For the case of TCP composites, TCP induced a reduction of T_{onset}, (inset Fig. 4(b)), as observed by Ferri et al. [39], attributing this behavior to the high hydrophilicity of TCP that induces hydrolytic cleavage of the PLA chains. However, this possible hydrolytic degradation in PLA/TCP composites leads to negligible modifications in the structural and thermal behavior of our composites. Huang et al. [40] observed similar behavior related to T_{onset} reduction induced by the addition of both HA and TCP in polycaprolactone (PCL) matrix. Since the operating temperature for these materials is in the range of 180–200 °C, the reductions shown are not significant.

Scaffolds are temporary templates for cell and tissue growth, and, specific features as adequate morphology, mechanical properties, and a suitable environment for cell spread, colonization, and tissue growth are required. The following section provides an in-depth analysis of scaffolds morphology, which exhibited a high level of printing accuracy related to the 3D model.

3.3. Morphological analysis

Scaffolds porosity and interconnectivity are essential attributes in the biological performance since they not only influence the mechanical properties of the constructs but also play a significant role in cell adhesion, proliferation, and vascularization [41,42]. The literature refers that the ideal scaffold architecture for bone tissue engineering capable of promoting cell adhesion, growth, and tissue regeneration is desired to have pores in the order of 150–500 μm in diameter and interconnected porosity of 60–80% [43–45]. However, porous in the range of 150–250 μm presents similar mechanical behavior [19]. As shown in Table 5, the scaffolds with geometry 0–90° and 0–45° presented theoretical porosity of 36% and 32%, respectively, and 100% of

Table 4
TGA results for PLA, PLA/HA, and PLA/TCP composites.

	T_{onset} (°C)*	T_{peak} (°C)*	Weight change RT to 200 °C* (%)	Residue (%)*
PLA	355.7 ± 2.1	381.8 ± 2.7	0.14 ± 0.09	0.4 ± 0.1
PLA5HA	359.0 ± 1.6	382.8 ± 2.8	0.06 ± 0.03	6.2 ± 0.8
PLA10HA	359.6 ± 0.2	384.9 ± 0.3	0.09 ± 0.01	9.3 ± 0.2
PLA5TCP	353.4 ± 2.9	379.7 ± 4.4	0.09 ± 0.01	4.9 ± 0.6
PLA10TCP	351.9 ± 0.5	376.2 ± 1.9	0.08 ± 0.01	9.5 ± 3.0

* Total mean ± standard deviation.

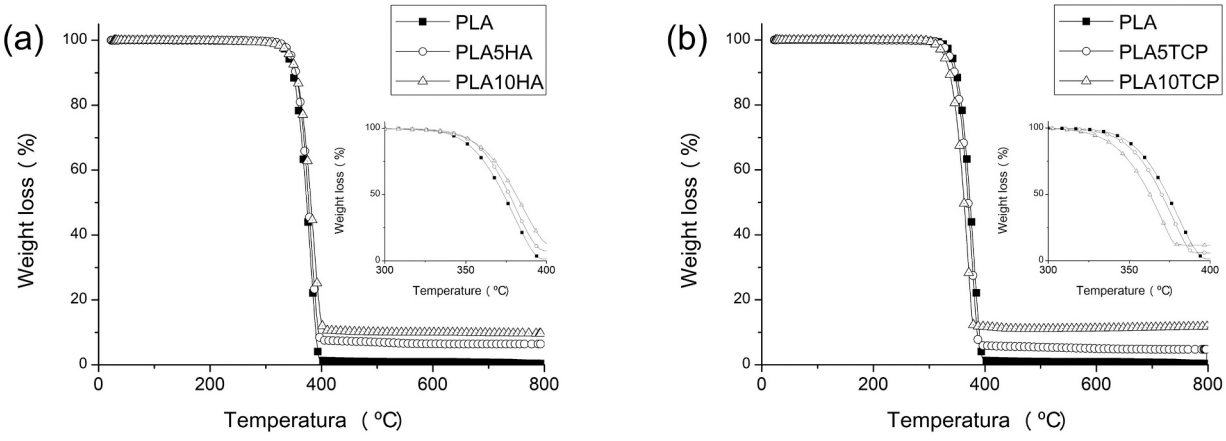

Fig. 4. Weight loss against temperature for (a) PLA and PLA/HA, (b) PLA and PLA/TCP.

Table 5
Micro-CT results of PLA, PLA/HA, and PLA/TCP bioactive scaffolds.

Samples	Porosity (%)			
	0–45° geometry		0–90° geometry	
	Scaffolds	Theoretical	Scaffolds	Theoretical
PLA	42 ± 2		39 ± 3	
5HA	46 ± 3		42 ± 5	
10HA	42 ± 5	32	45+ 4	36
5TCP	42 ± 3		40 ± 2	
10TCP	39 ± 3		43 ± 3	

interconnectivity. The micro-CT was used to evaluate the morphology of the scaffolds, and the data collected revealed a high level of precision since the values of porosity obtained are near to calculated by SolidWorks. In our scaffolds, 200 μm pore size were chosen attempting to improve cell attachment, and in contrast, a reduction in the overall porosity was obtained.

Fig. 5 presents the Micro-CT reconstructed 3D images from PLA scaffolds for both geometries. Fig. 5(a) and (b) show the reconstructed images of the scaffold with geometry 0–90°, while Fig. 5(c) presents the porosity presented in the same scaffold. Fig. 5(d–f) are the equivalent reconstructed images of the PLA scaffold with geometry 0–45°. The architecture of the scaffold is presented in Fig. 6, and Table 7 exhibits the morphological measurements. The morphology of the scaffolds was evaluated by two approaches for both geometries, analyzing the top view and the cross-section of fractured samples, and the geometries were highly reproducible in comparison to the geometries projected via SolidWorks® and to the results obtained of the reconstructed models independently of the addition of HA or TCP up to 10 wt%.

Another aspect that marginally reduces the printing precision is the thickness control of the filaments, which was outlined by only using the amount of the filament required for each printing and measuring it ten times alongside the length and two times each point to diminish minor

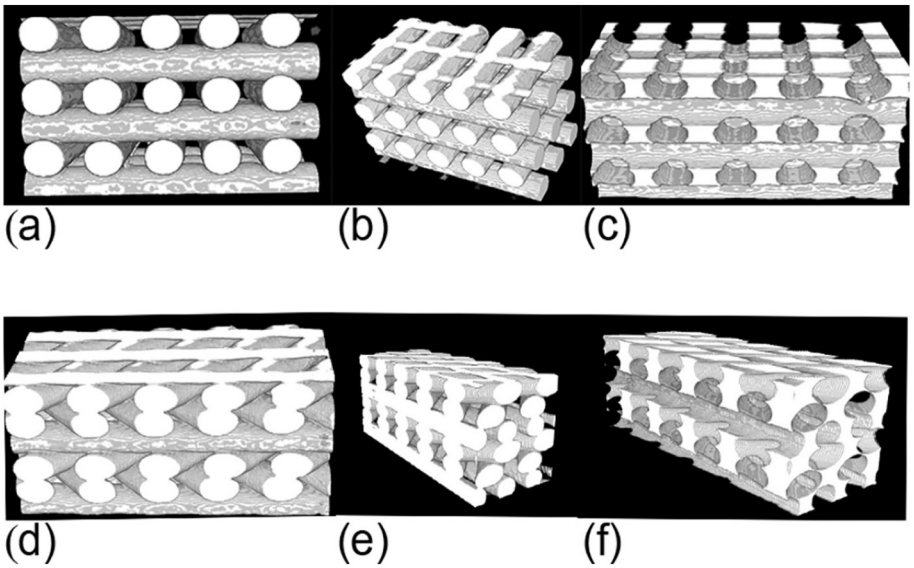

Fig. 5. Micro-CT reconstructs images illustrating the structural features of the PLA printed scaffolds. (a–c) 0–90° geometry and (d–f) 0–45° geometry. (a and d) lateral view; (b and e) angular view; (c and f) negative view, i.e., showing in white the empty space.

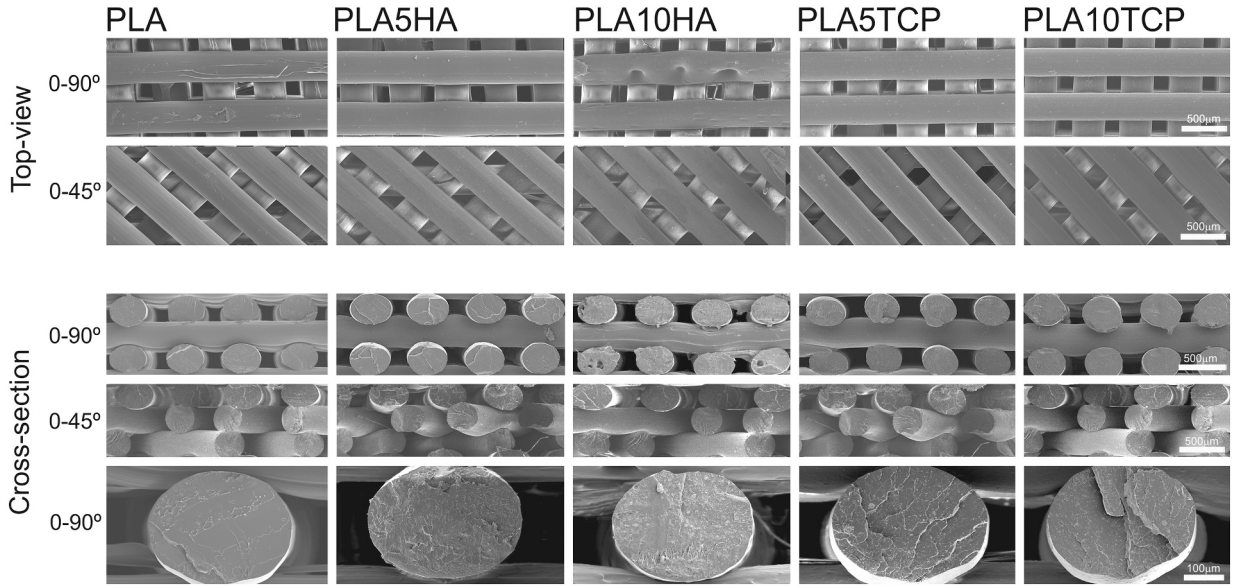

Fig. 6. Micrographs of scaffolds obtained by SEM analysis. Top-view and cross-section of PLA, PLA/HA, and PLA/TCP composites (magnifications of 50× and 200×).

Table 6
Morphological measurements of the scaffolds of PLA, PLA/HA, and PLA/TCP.

		Pore size (μm)	Filament width (μm)	Layer height (μm)
0–90° geometry	PLA	197 ± 14	376 ± 12	307 ± 15
	PLA5HA	175 ± 15	396 ± 10	297 ± 7
	PLA10HA	178 ± 16	395 ± 26	293 ± 10
	PLA5TCP	184 ± 27	402 ± 16	316 ± 13
	PLA10TCP	181 ± 12	406 ± 18	270 ± 20
0–45° geometry	PLA	183 ± 15	389 ± 12	302 ± 15
	PLA5HA	214 ± 16	384 ± 14	307 ± 23
	PLA10HA	183 ± 20	386 ± 17	280 ± 16
	PLA5TCP	204 ± 12	381 ± 19	306 ± 20
	PLA10TCP	206 ± 13	379 ± 14	300 ± 20

Table 7
Elastic modulus of the PLA, PLA/HA, and PLA/TCP samples*.

	Samples	Elastic modulus (MPa)*
100% Filled	PLA	82.1 ± 1.7
	PLA5HA	82.5 ± 1.2
	PLA10HA	78.5 ± 2.0
	PLA5TCP	83.3 ± 1.6
	PLA10TCP	79.6 ± 0.5
0–90° Geometry	PLA	67.8 ± 3.4
	PLA5HA	64.7 ± 5.7
	PLA10HA	71.7 ± 1.0
	PLA5TCP	68.9 ± 3.4
	PLA10TCP	65.9 ± 3.4
0–45° Geometry	PLA	70.4 ± 1.6
	PLA5HA	70.3 ± 1.9
	PLA10HA	68.7 ± 1.0
	PLA5TCP	69.3 ± 1.0
	PLA10TCP	68.0 ± 2.2

* Total mean ± standard deviation; # when compared with the respective 100% filled sample.

ovality effects from the extrusion process. Some authors noticed that filler content higher than 10 wt% leads to printing and extrusion problems, as clogging and filler accumulation in the nozzle [21,22].

However, these minor changes do not compromise the performance of the scaffolds for biomedical applications. EDS mapping was performed in the cross-section surface of the filaments aiming to investigate the HA and TCP distribution inside the filament (Supplementary data Fig. 6.1). The printing process, which involves elevated temperature and shear rate, leads to HA and TCP good dispersion inside the cross-section of the filaments, and higher intensity of the signal was obtained in some regions were the HA or TCP were present in higher concentrations (Table 6).

3.4. Mechanical properties

The developed scaffolds were tested under compressive load, which simulates in some extension the conditions imposed by the body during use, i.e., bone graft. Table 7 presents the elastic modulus of the three different geometries fabricated, namely, 100% filled, 0–90°, and 0–45°. Fig. 6.2 (Supplementary material) presents compressive stress-strain curves for 100% filled and 0–90° samples and the regions used for elastic modulus determination.

The samples PLA10HA and PLA10TCP with 100% filled presented a slight decrease in compressive modulus compared to PLA, however, only for PLA10HA it is statistically significant ($p < 0.05$). One possible explication for this is cooling ratio reduction since heated filaments are deposited side by side and kept at high temperatures during a longer time, similar behavior was observed in the PLA10HA samples [21].

Furthermore, for the composites, the filaments have their molecular mass reduced by the addition of HA and TCP (higher reduction for HA) during the printing process.

0–45° and 0–90° geometries presented mechanical properties 15–20% lower compared to their 100% filled references and an elastic modulus in the range of 65–72 MPa matching the required mechanical properties for cancellous bone grafts under compression [44,46]. However, 0–45° and 0–90° geometries did not exhibited statistical significance ($p < 0.8$) between groups, although the composite PLA10HA 0–90° geometry presented the highest value of elastic modulus. The elastic modulus obtained for PLA and composites is also consistent with other results presented in the literature, and as expected, the fabrication of porous geometries reduced elastic modulus [47,48].

It is worth noticing that for scaffolds and samples 100% filled, the tests were performed until the maximum load of 2 kN without failure, and it comprises a maximum compressive strength in the range of 10–11 MPa, which is compatible with human bone properties [49].

3.5. In vitro bioactivity via SBF

The bioactivity of the produced scaffolds was evaluated by soaking them in simulated body fluid (SBF) and analyzing the formation of new calcium phosphates in their surface. The SBF testing assay is usually the first approach to evaluate the capability of the material to be used in bone tissue engineering and the obtained results are illustrated in the images depicted in Fig. 7 [10,50,51]. It was observed that the composite scaffolds developed with PLA/HA and PLA/TCP filaments were capable of inducing the development of new calcium phosphates in their surface after soaking the samples in SBF for 7 days. On the contrary, since PLA is not bioactive, no calcium phosphates formation was observed in the surface of the scaffolds produced with bare PLA [50,51]. The obtained results suggest that both HA and TCP, due to its bioactive properties,

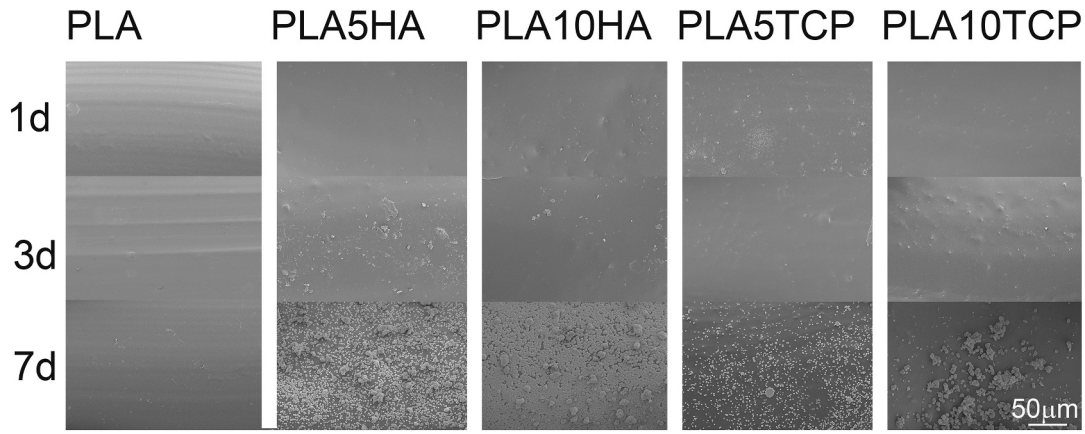

Fig. 7. Surface morphology of PLA, PLA/HA, and PLA/TCP scaffolds soaked under different times in SBF (magnification 500×).

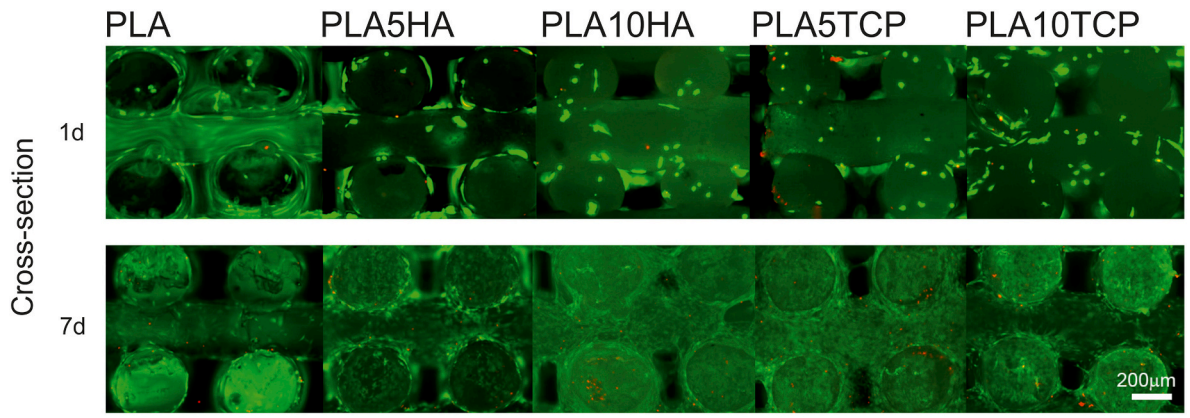

Fig. 8. Live/Dead cell viability assay for PLA, PLA/HA, and PLA/TCP scaffolds after 1 and 7 days of MC3T3 culture (magnification of 100×).

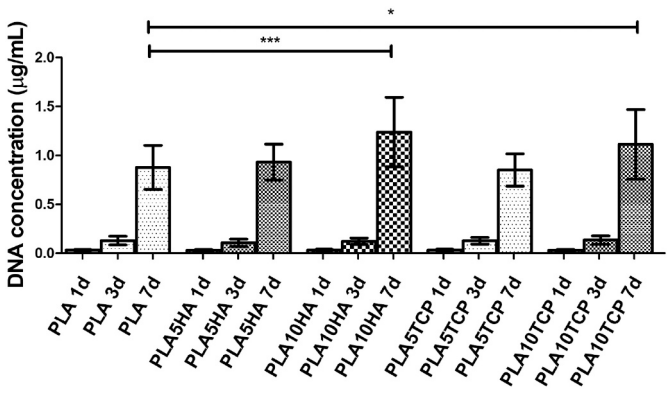

Fig. 9. DNA concentration over cell culture time on PLA, PLA/HA, and PLA/TCP scaffolds seeded with preosteoblast cells (*$p < 0.01$, ***$p < 0.0001$).

unleashed the formation of calcium phosphates in the surface of the scaffolds and particularly for HA composites, it was possible to observe the formation of a thicker layer of several small calcium phosphates particles upon 7 days of incubation in SBF.

3.6. Cell culture assays

One of the most successful approaches for developing devices for tissue engineering is the use of biodegradable and biocompatible materials. However, further studies also showed that physicochemical properties, as well as mechanical properties, surface roughness, volume, and pore size, also impact in the cell attachment, proliferation, and differentiation rate [52–56]. In the face of this, the fabrication of 3D scaffolds with well-controlled geometry using FFF and bioactive materials, namely, PLA combined with bioactive fillers (HA and TCP), makes them suitable materials for translational medical applications. Fig. 8 presents Live dead viability assay for PLA, PLA/HA, and PLA/TCP for 1 and 7 days, and as it can be seen, using a top-down approach for cell

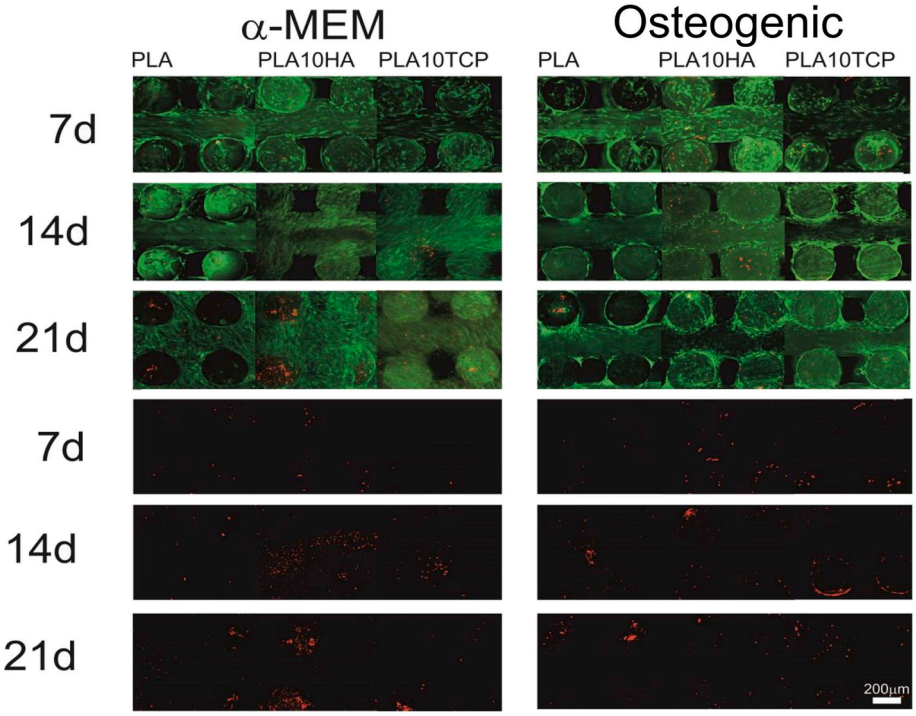

Fig. 10. Live/Dead cell viability assay for PLA, PLA10HA, and PLA10TCP scaffolds after 7, 14, and 21 days with and without osteogenic medium. The red signal (dead cells) is showed as a separated channel at the bottom of the figure for each time-point (magnification of 100×).

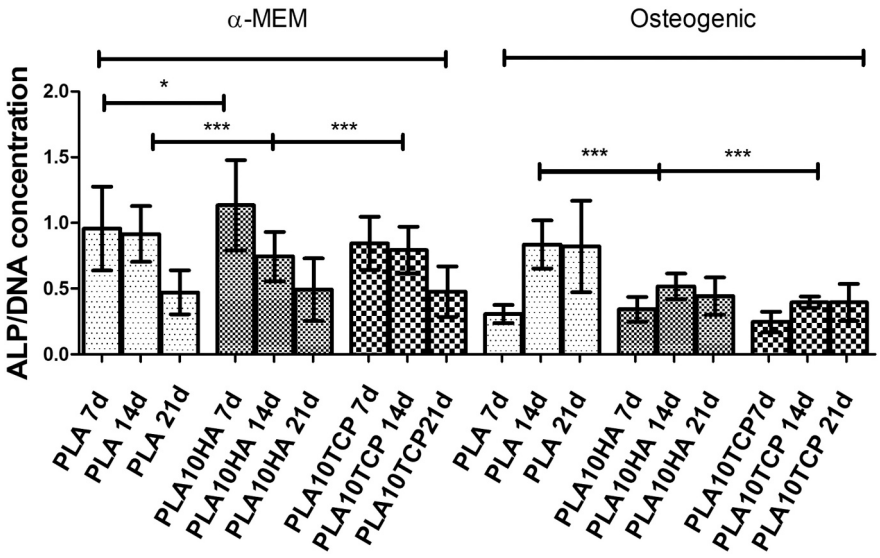

Fig. 11. ALP/DNA concentration over cell culture time for PLA, PLA10HA, and PLA10TCP scaffolds seeded with hASCs cells with and without the osteogenic elements (*$p < 0.01$, ***$p < 0.0001$).

seeding, firstly, the cells attached to the surface then later spread and colonized the internal portion of the scaffolds. It is essential to notice that the selection of adequate pore size also aids cell attachment and proliferation [19]. Since the developed geometries presented comparable mechanical properties and porosity, the authors decided to perform cytocompatibility and differentiation tests only in 0–90° geometry since this geometry has been more investigated.

The scaffolds presented a suitable environment that allowed cell proliferation and spread in a short period. It was observed in the scaffold PLA10HA, after 7 days of culture, a high cell confluence, and in some points, the pores of the scaffolds were nearly closed by cells. Recent studies also showed the bioactivity capacity of the combination of PLA/HA, even using HA as a coating instead of mixed within the polymeric matrix, wherein an increase in cell proliferation and bone ingrowth without inflammation has been observed [11,20,57]. The scaffolds with 5 and 10 wt% of TCP also supported intensified cell spreading and colonization.

DNA quantification was performed to corroborate the qualitative live/dead assay and evaluate cell proliferation in the developed scaffolds. It was observed no noteworthy differences in the DNA concentration between the PLA, PLA/HA, and PLA/TCP constructs for the short periods of analyses (1 and 3 days) (Fig. 9). It seems that cell spreading and proliferation required longer times to experience significant variation, as seen in the difference of morphology between the samples from 1 and 7 days in Fig. 8. In fact, after 7 days of cell culture, the samples PLA10HA and PLA10TCP demonstrated a significantly higher amount of DNA when compared with the PLA, PLA5HA, and PLA5TCP sample ($p < 0.01$ and $p < 0.001$, respectively). However, no statistical difference was observed between PLA10HA and PLA10TCP. Such a result indicates that the higher concentrations of both HA and TCP could guide a good cellular response by increasing material cytocompatibility [16,19,57].

Since the scaffolds PLA10HA and PLA10TCP showed high biocompatibility with improved cell proliferation in contact with MC3T3-E1 cells, we proceeded with a culture test with those compositions using hASCs. Fig. 10 presents Live/Dead viability assay for PLA, PLA10HA, and PLA10TCP for 7, 14, and 21 days using hASCs with and without differentiation medium. It was possible to observe that for 7 days of culture, both the PLA and the PLA10HA and PLA10TCP biocomposites showed similar proliferation, including using the two different culture mediums. For 14 days assay, greater proliferation was observed for PLA10HA and PLA10TCP cultured in α-MEM. In those samples, a more intense red signal (channel separated at the bottom of the figure) is also observed, indicating that as more cells proliferate, they are also under more stress and may die. For samples with osteogenic culture medium, the addition of components that induce cell differentiation reduces cell proliferation, and therefore they tend to differentiate [58]. Lastly, for samples culture in 21 days in α-MEM, extensive proliferation is observed since the pores of the scaffolds are practically closed, and leading to an intensification of the number of dead cells (red signal). In samples cultured in osteogenic medium, a greater proliferation of cells is observed over 21 days period; however, in a smaller amount than those tested in α-MEM. As expected, cell-cultured in basal medium exhibited higher cell density than those cultured in the differentiation medium [29].

The growth and differentiation of osteoblasts are characterized by three main events in the extracellular matrix: (i) proliferation, (ii) maturation, and (iii) mineralization [59]. The formation of ALP can evaluate mineralization, and this enzyme exists in several tissues and has a role in forming hard tissues. ALP acts in the early stages of bone mineralization, and it is widely reported that once it reaches its mineralization onset (usually 14 days), there is a decrease in its expression [59].

Fig. 11 shows the concentration of ALP/DNA for different cell culture times with and without osteogenic elements. Samples cultured in α-MEM, the peak of ALP occurs for 7 days and suffer a decrease for longer culture times. The PLA10HA ($p < 0.01$ compared to PLA) showed a high expression of ALP/DNA, and its values decrease more rapidly than for PLA and PLA10TCP [60]. While the samples in the osteogenic medium, the samples presented low expression of ALP/DNA at 7 days, and for the neat PLA presented a higher expression compared to PLA10HA and PLA10TCP for 14 and 21 days ($p < 0.0001$). Samples cultured in the osteogenic medium showed ALP peak in 14 days and remained constant until 21 days.

Nakagawa et al. [61] investigated the biological effects of TCP microparticles at different concentrations in the proliferation, cytotoxicity, and calcification of human synovial mesenchymal stem cells. Microparticles at a concentration of 1.0 mg mL^{-1} of TCP significantly inhibited proliferation and increased the number of dead cells, while at lower concentrations, such as 0.1 mg mL^{-1} TCP promoted calcification of the cells. Similar results were obtained by Li et al. [62] with the use of HA nanoparticles in high concentrations (from 40 to 200 μg of particles per mL of medium). According to the authors, HA nanoparticles decreased the concentrations of calcium and phosphate in the culture medium instead of increasing them, and this may be a result of the

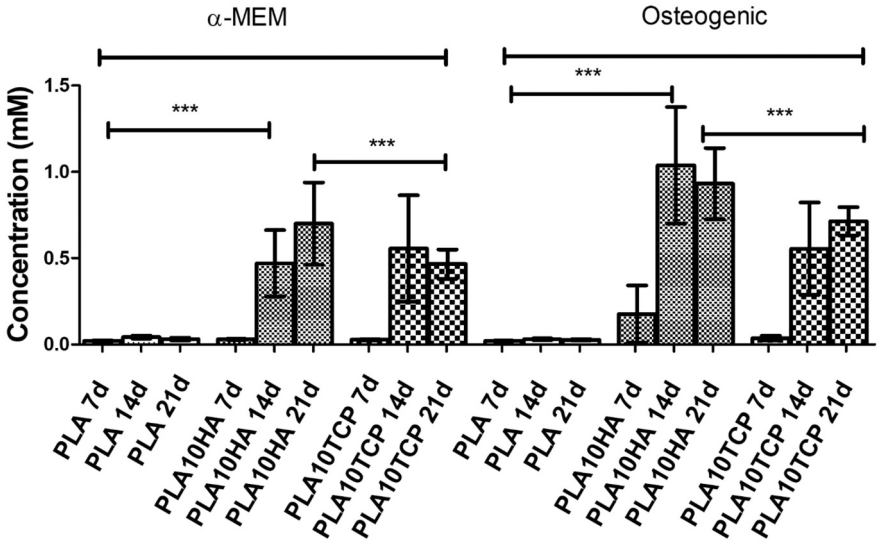

Fig. 12. PLA, PLA10HA, and PLA10TCP scaffolds after 14 d cultured in osteogenic medium (a). AR concentration in mM for PLA scaffolds and PLA/HA and PLA/TCP biocomposites grown with hASCs under different culture times, 7, 14 and 21 days (b) (***$p < 0.0001$).

absorption of calcium and phosphate ions on the surface of the HA during the process of crystalline growth and mineralization. However, for lower concentrations, HA nanoparticles promoted cell growth due to the absorption of proteins and the binding of these cells to the surface of HA.

However, some authors show that although ALP is widely used to determine osteogenic differentiation, considering only this value may be a premature conclusion [63]. Thus, Alizarin Red (AR) was chosen as a complementary analysis of the mineralization of the scaffolds. AR is a pigment used to locate calcium deposits in tissues and is an indicator of the production of mineralized extracellular matrix by mature osteoblastic cells [64]. Additionally, calcium and phosphorus can promote the mineralization of bone tissues [65]. Fig. 12 shows AR quantification for PLA, PLA10HA, and PLA10TCP scaffolds cultured with hASCs under different culture times.

As can be seen, the scaffolds of PLA10HA and PLA10TCP, due to the addition of calcium phosphates, HA, and TCP, respectively, had high levels of mineralization, whereas pure PLA shows only almost imperceptible traces without using a microscope.

The quantification of the scaffold mineralization was performed by destaining the samples with a solution of cetylpyridinium chloride (CPC). It is worth remembering that because scaffolds already have in their composition materials that can lead to spontaneous dyeing, tests were carried out on the scaffolds for the same culture times, however, without cells. In Fig. 12 the use of an osteogenic medium led to a much higher concentration of mineralized matrix, and the values were higher for the composition with HA, whereas for scaffolds with TCP, and there was a great evolution from 7 to 14 days and a small increase for 21 days. It is worth remembering that for the PLA10HA and PLA10TCP scaffolds, even without the addition of osteogenic medium, these samples showed potentiation of osteogenesis, although at a minor level compared to sample culture in the osteogenic medium.

Summarily, combining a biomimetic approach to bottom-up scaffolds manufactured with bioactive materials and adequate pore size assist cell proliferation and differentiation and its use in bone tissue engineering applications [19].

4. Conclusion

PLA, PLA/HA, and PLA/TCP scaffolds were successfully produced using twin-screw extrusion, followed by FFF technology to obtain 3D architectures with different geometries. All the extruded filaments presented suitable rheological and thermal properties for the fabrication of 3D scaffolds. According to the Micro-CT and SEM analyses, the scaffolds presented a high level of printing accuracy related to the 3D model. Moreover, the developed 3D architectures presented mechanical properties as adequate compressive modulus and compressive strength for bone graft applications ranging from 65–72 MPa and 10–11 MPa, respectively. The addition of HA and TCP become the scaffolds bioactive, stimulating new calcium phosphates upon incubation in SBF, which would allow an osteoblast friendly microenvironment. Moreover, the printed composite scaffolds supported cell attachment, proliferation, and differentiation. The reported methodology enables the production of bioactive scaffolds with well-controlled geometry by using 3D printer technology, with the potential to be used for bone grafts and bone tissue engineering..

CRediT authorship contribution statement

Eduardo H Backes: Conceptualization, Methodology, Investigation, Original draft preparation; **Emanuel M. Fernandes**: Supervision, Conceptualization, Review & Editing; **Gabriela S. Diogo**: Methodology, Investigation, Review & Editing; **Catarina F. Marques**: Methodology, Investigation, Review & Editing; **Tiago H. Silva**: Supervision, Conceptualization, Resources, Review & Editing; **Lidiane C. Costa**: Conceptualization, Resources, Review & Editing; **Fabio R. Passador**: Supervision, Conceptualization, Review & Editing; **Rui L. Reis**: Supervision, Conceptualization, Resources, Review & Editing; **Luiz A. Pessan**: Supervision, Conceptualization, Resources, Review & Editing.

Declaration of competing interest

The authors whose names are listed immediately below certify that they have NO affiliations with or involvement in any organization or entity with any financial interest (such as honoraria; educational grants; participation in speakers' bureaus; membership, employment, consultancies, stock ownership, or other equity interest; and expert testimony or patent-licensing arrangements), or non-financial interest (such as personal or professional relationships, affiliations, knowledge or beliefs) in the subject matter or materials discussed in this manuscript.

Acknowledgment

This study was financed in part by the Coordenação de

Aperfeiçoamento de Pessoal de Nível Superior - Brasil (CAPES) - Finance Code 001 and for the European Regional Development Fund (EFDR), under the scope of the INTERREG España-Portugal (POCTEP) project 0302_CVMAR_I_1_P. The authors would like to thanks the FAPESP (Process Number 2018/13625-2, 2017/11366-7 and 2017/09609-9), Catarina F. Marques thanks Fundação para a Ciência e a Tecnologia (FCT) for the contract CEECIND/04687/2017 and Emanuel M. Fernandes thanks to Structured Projects for the contract NORTE-01-0145-FEDER-000021. The authors would like to thank Professor Luiz Henrique Capparelli Mattoso, Dr. Paulo Renato Orlandi Lasso and Empresa Brasileira de Pesquisa Agropecuária (Embrapa) for Micro-CT analysis. The authors would like to thank Professor Silvia H. Bettini and Dra. Talita R. Rigolin for GPC analysis (FAPESP Process Number 2011/21313-1).

Appendix A. Supplementary data

Supplementary data to this article can be found online at https://doi.org/10.1016/j.msec.2021.111928.

References

[1] I. Armentano, M. Dottori, E. Fortunati, S. Mattioli, J.M. Kenny, Biodegradable polymer matrix nanocomposites for tissue engineering: a review, Polym. Degrad. Stab. 95 (2010) 2126–2146, https://doi.org/10.1016/j.polymdegradstab.2010.06.007.

[2] R.M. Rasal, A.V. Janorkar, D.E. Hirt, Progress in Polymer Science Poly(Lactic Acid) Modifications vol. 35, 2010, pp. 338–356, https://doi.org/10.1016/j.progpolymsci.2009.12.003.

[3] E. Castro-Aguirre, F. Iñiguez-Franco, H. Samsudin, X. Fang, R. Auras, Poly(lactic acid)—mass production, processing, industrial applications, and end of life, Adv. Drug Deliv. Rev. 107 (2016) 333–366, https://doi.org/10.1016/j.addr.2016.03.010.

[4] S. Farah, D.G. Anderson, R. Langer, Physical and mechanical properties of PLA, and their functions in widespread applications — a comprehensive review, Adv. Drug Deliv. Rev. 107 (2016) 367–392, https://doi.org/10.1016/j.addr.2016.06.012.

[5] A. Aimar, A. Palermo, B. Innocenti, The role of 3D printing in medical applications: a state of the art, J. Healthc. Eng. 2019 (2019) 1–10, https://doi.org/10.1155/2019/5340616.

[6] J. Akmal, M. Salmi, A. Mäkitie, R. Björkstrand, J. Partanen, Implementation of industrial additive manufacturing: intelligent implants and drug delivery systems, J. Funct. Biomater. 9 (2018) 41, https://doi.org/10.3390/jfb9030041.

[7] P. Ravi, P.S. Shiakolas, T.R. Welch, Poly-L-lactic acid: pellets to fiber to fused filament fabricated scaffolds, and scaffold weight loss study, Addit. Manuf. 16 (2017) 167–176, https://doi.org/10.1016/j.addma.2017.06.002.

[8] X. Wang, M. Jiang, Z.W. Zhou, J.H. Gou, D. Hui, 3D printing of polymer matrix composites: a review and prospective, Compos. B Eng. 110 (2017) 442–458, https://doi.org/10.1016/j.compositesb.2016.11.034.

[9] C. Liu, Z. Xia, J.T.T. Czernuszka, Design and development of three-dimensional scaffolds for tissue engineering, Chem. Eng. Res. Des. 85 (2007) 1051–1064, https://doi.org/10.1205/cherd06196.

[10] L. Siqueira, F.R.R. Passador, M.M.M. Costa, A.O.O. Lobo, E. Sousa, Influence of the addition of β-TCP on the morphology, thermal properties and cell viability of poly (lactic acid) fibers obtained by electrospinning, Mater. Sci. Eng. C 52 (2015) 135–143, https://doi.org/10.1016/j.msec.2015.03.055.

[11] H. Zhang, X. Mao, Z. Du, W. Jiang, X. Han, D. Zhao, D. Han, Q. Li, Three dimensional printed macroporous polylactic acid/hydroxyapatite composite scaffolds for promoting bone formation in a critical-size rat calvarial defect model, Sci. Technol. Adv. Mater. 17 (2016) 136–148, https://doi.org/10.1080/14686996.2016.1145532.

[12] C.M. Alves, Y. Yang, D. Marton, D.L. Carnes, J.L. Ong, L. Sylvia, D.D. Dean, R. L. Reis, C.M. Agrawal, Plasma surface modification of poly(D,L-lactic acid) as a tool to enhance protein adsorption and the attachment of different cell types, J. Biomed. Mater. Res. B Appl. Biomater. 87B (2008) 59–66, https://doi.org/10.1002/jbm.b.31068.

[13] S.V. Dorozhkin, Calcium orthophosphates, Biomatter. 1 (2011) 121–164, https://doi.org/10.4161/biom.18790.

[14] K. Rezwan, Q.Z. Chen, J.J. Blaker, A.R. Boccaccini, Biodegradable and bioactive porous polymer/inorganic composite scaffolds for bone tissue engineering, Biomaterials. 27 (2006) 3413–3431, https://doi.org/10.1016/j.biomaterials.2006.01.039.

[15] A.-M. Yousefi, H. Oudadesse, R. Akbarzadeh, E. Wers, A. Lucas-Girot, Physical and biological characteristics of nanohydroxyapatite and bioactive glasses used for bone tissue engineering, Nanotechnol. Rev. 3 (2014) 527–552, https://doi.org/10.1515/ntrev-2014-0013.

[16] I.A.W.B. Siqueira, N.K. de Moura, J.P. de Barros Machado, E.H. Backes, F. Roberto Passador, E. de Sousa Trichês, Porous membranes of the polycaprolactone (PCL) containing calcium silicate fibers for guided bone regeneration, Mater. Lett. 206 (2017), https://doi.org/10.1016/j.matlet.2017.07.011.

[17] F.S. Senatov, K.V. Niaza, A.A. Stepashkin, S.D. Kaloshkin, Low-cycle fatigue behavior of 3d-printed PLA-based porous scaffolds, Compos. Part B 97 (2016) 193–200, https://doi.org/10.1016/j.compositesb.2016.04.067.

[18] E. Zuza, E. Meaurio, J. Sarasua, Biodegradable polylactide-based composites, in: Composites From Renewable and Sustainable Materials, InTech, 2016.

[19] A. Grémare, V. Guduric, R. Bareille, V. Heroguez, S. Latour, N. L'heureux, J.-C. C. Fricain, S. Catros, D. Le Nihouannen, A. Gremare, V. Guduric, R. Bareille, V. Heroguez, S. Latour, N. L'heureux, J.-C.C. Fricain, S. Catros, D. Le Nihouannen, A. Grémare, V. Guduric, R. Bareille, V. Heroguez, S. Latour, N. L'heureux, J.-C. C. Fricain, S. Catros, D. Le Nihouannen, Characterization of printed PLA scaffolds for bone tissue engineering, J. Biomed. Mater. Res. A 106 (2018) 887–894, https://doi.org/10.1002/jbm.a.36289.

[20] K.V. Niaza, F.S. Senatov, A. Stepashkin, N.Y. Anisimova, M.V. Kiselevsky, Long-term creep and impact strength of biocompatible 3D-printed PLA-based scaffolds, Nano Hybrids Compos. 13 (2017) 15–20, https://doi.org/10.4028/www.scientific.net/NHC.13.15.

[21] C. Amnael Orozco-Díaz, R. Moorehead, G.C. Reilly, F. Gilchrist, C. Miller, Characterization of a composite polylactic acid-hydroxyapatite 3D-printing filament for bone-regeneration, Biomed. Phys. Eng. Express 6 (2020), 025007, https://doi.org/10.1088/2057-1976/ab73f8.

[22] D. Wu, A. Spanou, A. Diez-Escudero, C. Persson, 3D-printed PLA/HA composite structures as synthetic trabecular bone: a feasibility study using fused deposition modeling, J. Mech. Behav. Biomed. Mater. 103 (2020) 103608, https://doi.org/10.1016/j.jmbbm.2019.103608.

[23] X. Chen, C. Gao, J. Jiang, Y. Wu, P. Zhu, G. Chen, 3D printed porous PLA/nHA composite scaffolds with enhanced osteogenesis and osteoconductivity in vivo for bone regeneration, Biomed. Mater. 14 (2019), 065003, https://doi.org/10.1088/1748-605X/ab388d.

[24] R. Donate, M. Monzón, Z. Ortega, L. Wang, V. Ribeiro, D. Pestana, J.M. Oliveira, R. L. Reis, Comparison between calcium carbonate and β-tricalcium phosphate as additives of 3D printed scaffolds with polylactic acid matrix, J. Tissue Eng. Regen. Med. (2019), term.2990, https://doi.org/10.1002/term.2990.

[25] T. Sui, E. Salvati, H. Zhang, K. Nyaza, F.S. Senatov, A.I. Salimon, A.M. Korsunsky, Probing the complex thermo-mechanical properties of a 3D-printed polylactide-hydroxyapatite composite using in situ synchrotron X-ray scattering, J. Adv. Res. 16 (2019) 113–122, https://doi.org/10.1016/j.jare.2018.11.002.

[26] V.H. Sangeetha, H. Deka, T.O. Varghese, S.K. Nayak, State of the art and future prospectives of poly(lactic acid) based blends and composites, Polym. Compos. 39 (2018) 81–101, https://doi.org/10.1002/pc.23906.

[27] L.P. da Silva, M.T. Cerqueira, R.A. Sousa, R.L. Reis, M. Correlo, A.P. Marques, Engineering cell-adhesive gellan gum spongy-like hydrogels for regenerative medicine purposes, Acta Biomater. 10 (2014) 4787–4797, https://doi.org/10.1016/j.actbio.2014.07.009.

[28] M.T. Cerqueira, R.P. Pirraco, T.C. Santos, D.B. Rodrigues, A.M. Frias, A.R. Martins, R.L. Reis, A.P. Marques, Human adipose stem cells cell sheet constructs impact epidermal morphogenesis in full-thickness excisional wounds, Biomacromolecules 14 (2013) 3997–4008, https://doi.org/10.1021/bm4011062.

[29] G. Diogo, E. López-Senra, R. Pirraco, R. Canadas, E. Fernandes, J. Serra, R. Pérez-Martín, C. Sotelo, A. Marques, P. González, J. Moreira-Silva, T. Silva, R. Reis, Marine collagen/apatite composite scaffolds envisaging hard tissue applications, Mar. Drugs 16 (2018) 269, https://doi.org/10.3390/md16080269.

[30] S.F.F. Costa, F.M.M. Duarte, J.A.A. Covas, Estimation of filament temperature and adhesion development in fused deposition techniques, J. Mater. Process. Technol. 245 (2017) 167–179, https://doi.org/10.1016/j.jmatprotec.2017.02.026.

[31] P.-L. Lin, H.-W. Fang, T. Tseng, W.-H. Lee, Effects of hydroxyapatite dosage on mechanical and biological behaviors of polylactic acid composite materials, Mater. Lett. 61 (2007) 3009–3013, https://doi.org/10.1016/j.matlet.2006.10.064.

[32] Y. Fan, H. Nishida, S. Hoshihara, Y. Shirai, Y. Tokiwa, T. Endo, Pyrolysis kinetics of poly(L-lactide) with carboxyl and calcium salt end structures, Polym. Degrad. Stab. 79 (2003) 547–562, https://doi.org/10.1016/S0141-3910(02)00374-9.

[33] E.H. Backes, L. de N. Pires, L.C. Costa, F.R. Passador, L.A. Pessan, Analysis of the degradation during melt processing of PLA/Biosilicate® composites, J. Compos. Sci. 3 (2019) 52, https://doi.org/10.3390/jcs3020052.

[34] E.H. Backes, L. de Nóbile Pires, H.S. Selistre-de-Araujo, L.C. Costa, F.R. Passador, L. A. Pessan, Development and characterization of printable PLA/β-TCP bioactive composites for bone tissue applications, J. Appl. Polym. Sci. (2020) 49759, https://doi.org/10.1002/app.49759.

[35] I.S. Zope, A. Dasari, G. Camino, Elucidating the catalytic effect of metal ions in montmorillonite on thermal degradation of organic modifier, Mater. Chem. Phys. 157 (2015) 69–79, https://doi.org/10.1016/j.matchemphys.2015.03.015.

[36] C. Esposito Corcione, F. Gervaso, F. Scalera, F. Montagna, A. Sannino, A. Maffezzoli, The feasibility of printing polylactic acid-nanohydroxyapatite composites using a low-cost fused deposition modeling 3D printer, J. Appl. Polym. Sci. 134 (2017) 1–10, https://doi.org/10.1002/app.44656.

[37] J. Ferreira, A. Gloria, S. Cometa, J.F.J.J. Coelho, M. Domingos, Effect of in vitro enzymatic degradation on 3D printed poly(epsilon-caprolactone) scaffolds: morphological, chemical and mechanical properties, J. Appl. Biomat. Funct. Mater. 15 (2017) E185–E195, https://doi.org/10.5301/jabfm.5000363.

[38] A.J. Salgado, Y.M. Wang, J.F. Mano, R.L. Reis, Influence of molecular weight and crystallinity of poly(L-lactic acid) on the adhesion and proliferation of human osteoblast like cells, Mater. Sci. Forum 514–516 (2006) 1020–1024, https://doi.org/10.4028/www.scientific.net/MSF.514-516.1020.

[39] J. Ferri, I. Gisbert, D. García-Sanoguera, M. Reig, R. Balart, The effect of beta-tricalcium phosphate on mechanical and thermal performances of poly(lactic acid), J. Compos. Mater. 50 (2016) 4189–4198, https://doi.org/10.1177/0021998316636205.

[40] B. Huang, G. Caetano, C. Vyas, J.J. Blaker, C. Diver, P. Bártolo, Polymer-ceramic composite scaffolds: the effect of hydroxyapatite and β-tri-calcium phosphate, Materials. 11 (2018) 129, https://doi.org/10.3390/ma11010129.
[41] A. Wubneh, E.K. Tsekoura, C. Ayranci, H. Uludağ, Current state of fabrication technologies and materials for bone tissue engineering, Acta Biomater. 80 (2018) 1–30, https://doi.org/10.1016/j.actbio.2018.09.031.
[42] T. Serra, J.A. Planell, M. Navarro, High-resolution PLA-based composite scaffolds via 3-D printing technology, Acta Biomater. 9 (2013) 5521–5530, https://doi.org/10.1016/j.actbio.2012.10.041.
[43] I. Denry, L.T. Kuhn, Design and characterization of calcium phosphate ceramic scaffolds for bone tissue engineering, Dent. Mater. 32 (2016) 43–53, https://doi.org/10.1016/j.dental.2015.09.008.
[44] A. Kumar, S. Mandal, S. Barui, R. Vasireddi, U. Gbureck, M. Gelinsky, B. Basu, Low temperature additive manufacturing of three dimensional scaffolds for bone-tissue engineering applications: processing related challenges and property assessment, Mater. Sci. Eng. R. Rep. 103 (2016) 1–39, https://doi.org/10.1016/j.mser.2016.01.001.
[45] S.S.V. Dorozhkin, Bioceramics of calcium orthophosphates, Biomaterials 31 (2010) 1465–1485, https://doi.org/10.1016/j.biomaterials.2009.11.050.
[46] A.R. Boccaccini, J.J. Blaker, Bioactive composite materials for tissue engineering scaffolds, Expert Rev. Med. Devic. 2 (2005) 303–317, https://doi.org/10.1586/17434440.2.3.303.
[47] A. Gregor, E. Filová, M. Novák, J. Kronek, H. Chlup, M. Buzgo, V. Blahnová, V. Lukášová, M. Bartoš, A. Nečas, J. Hošek, Designing of PLA scaffolds for bone tissue replacement fabricated by ordinary commercial 3D printer, J. Biol. Eng. 11 (2017) 31, https://doi.org/10.1186/s13036-017-0074-3.
[48] L.R. Jaidev, K. Chatterjee, Surface functionalization of 3D printed polymer scaffolds to augment stem cell response, Mater. Des. 161 (2019) 44–54, https://doi.org/10.1016/j.matdes.2018.11.018.
[49] C.E. Misch, Z. Qu, M.W. Bidez, Mechanical properties of trabecular bone in the human mandible: implications for dental implant treatment planning and surgical placement, J. Oral Maxillofac. Surg. 57 (1999) 700–706, https://doi.org/10.1016/S0278-2391(99)90437-8.
[50] J. Roether, A. Boccaccini, L. Hench, V. Maquet, S. Gautier, R. Jérôme, Development and in vitro characterisation of novel bioresorbable and bioactive composite materials based on polylactide foams and Bioglass® for tissue engineering applications, Biomaterials 23 (2002) 3871–3878, https://doi.org/10.1016/S0142-9612(02)00131-X.
[51] Z. Hong, R.L. Reis, J.F. Mano, Preparation and in vitro characterization of scaffolds of poly(l-lactic acid) containing bioactive glass ceramic nanoparticles, Acta Biomater. 4 (2008) 1297–1306, https://doi.org/10.1016/j.actbio.2008.03.007.
[52] D. Li, J. Zhou, F. Chowdhury, J. Cheng, N. Wang, F. Wang, Role of mechanical factors in fate decisions of stem cells, Regen. Med. 6 (2011) 229–240, https://doi.org/10.2217/rme.11.2.
[53] G. Hannink, J.J.C. Arts, Bioresorbability, porosity and mechanical strength of bone substitutes: what is optimal for bone regeneration? Injury 42 (2011) S22–S25, https://doi.org/10.1016/j.injury.2011.06.008.
[54] F. Kabirian, B. Ditkowski, A. Zamanian, R. Heying, M. Mozafari, An innovative approach towards 3D-printed scaffolds for the next generation of tissue-engineered vascular grafts, Mater. Today Proc. 5 (2018) 15586–15,594, https://doi.org/10.1016/j.matpr.2018.04.167.
[55] J.F.M. Ribeiro, S.M. Oliveira, J.L. Alves, A.J. Pedro, R.L. Reis, E.M. Fernandes, J. F. Mano, Structural monitoring and modeling of the mechanical deformation of three-dimensional printed poly(ε-caprolactone) scaffolds, Biofabrication 9 (2017), 025015, https://doi.org/10.1088/1758-5090/aa698e.
[56] G. Criscenti, A. Longoni, A. Di Luca, C. De Maria, C.A. Van Blitterswijk, G. Vozzi, L. Moroni, Triphasic scaffolds for the regeneration of the bone-ligament interface, Biofabrication 8 (2016) 15009, https://doi.org/10.1088/1758-5090/8/1/015009.
[57] A. Liu, G. Xue, M. Sun, H. Shao, C. Ma, Q. Gao, Z. Gou, S. Yan, Y. Liu, Y. He, 3D printing surgical implants at the clinic: a experimental study on anterior cruciate ligament reconstruction, Sci. Rep. 6 (2016) 21704, https://doi.org/10.1038/srep21704.
[58] S. Ruijtenberg, S. van den Heuvel, Coordinating cell proliferation and differentiation: antagonism between cell cycle regulators and cell type-specific gene expression, Cell Cycle 15 (2016) 196–212, https://doi.org/10.1080/15384101.2015.1120925.
[59] D.R. Fonseca, R. Sobreiro-Almeida, P.C. Sol, N.M. Neves, Development of non-orthogonal 3D-printed scaffolds to enhance their osteogenic performance, Biomater. Sci. 6 (2018) 1569–1579, https://doi.org/10.1039/C8BM00073E.
[60] W. Yang, L. Long, R. Wang, D. Chen, S. Duan, F. Xu, Surface-modified hydroxyapatite nanoparticle-reinforced polylactides for three-dimensional printed bone tissue engineering scaffolds, J. Biomed. Nanotechnol. 14 (2018) 294–303, https://doi.org/10.1166/jbn.2018.2495.
[61] Y. Nakagawa, T. Muneta, K. Tsuji, S. Ichinose, Y. Hakamatsuka, H. Koga, I. Sekiya, β-Tricalcium phosphate micron particles enhance calcification of human mesenchymal stem cells in vitro, J. Nanomater. (2013) 1–13, https://doi.org/10.1155/2013/426786.
[62] Y. Liu, G. Wang, Y. Cai, H. Ji, G. Zhou, X. Zhao, R. Tang, M. Zhang, In vitro effects of nanophase hydroxyapatite particles on proliferation and osteogenic differentiation of bone marrow-derived mesenchymal stem cells, J. Biomed. Mater. Res. A 90A (2009) 1083–1091, https://doi.org/10.1002/jbm.a.32192.
[63] M.D. Weir, H.H.K. Xu, Osteoblastic induction on calcium phosphate cement-chitosan constructs for bone tissue engineering, J. Biomed. Mater. Res. A 94A (2010) 223–233, https://doi.org/10.1002/jbm.a.32665.
[64] I.A.W.B. Siqueira, S.S. Amaral, N.K. de Moura, J.P.B. Machado, E.H. Backes, F. R. Passador, S.E.A. Camargo, L.M.R. de Vasconcellos, E.S. Trichês, In vitro bioactivity and biological assays of porous membranes of the poly(lactic acid) containing calcium silicate fibers, Polym. Bull. (2019), https://doi.org/10.1007/s00289-019-03021-5.
[65] Y.-L. Chang, C.M. Stanford, J.C. Keller, Calcium and phosphate supplementation promotes bone cell mineralization: implications for hydroxyapatite (HA)-enhanced bone formation, J. Biomed. Mater. Res. 52 (2000) 270–278, https://doi.org/10.1002/1097-4636(200011)52:2<270::AID-JBM5>3.0.CO;2-1.